INTERNATIONAL JOURNAL FOR NUMERICAL METHODS IN FLUIDS
Int. J. Numer. Meth. Fluids 2005; **49**:721–737
Published online 26 July 2005 in Wiley InterScience (www.interscience.wiley.com). DOI: 10.1002/fld.1019

A semi-implicit finite element model for non-hydrostatic (dispersive) surface waves

Roy A. Walters*,†

National Institute for Water and Atmospheric Research, P.O. Box 8602, Christchurch, New Zealand

SUMMARY

The objective of this research is to develop a model that will adequately simulate the dynamics of tsunami propagating across the continental shelf. In practical terms, a large spatial domain with high resolution is required so that source areas and runup areas are adequately resolved. Hence efficiency of the model is a major issue. The three-dimensional Reynolds averaged Navier–Stokes equations are depth-averaged to yield a set of equations that are similar to the shallow water equations but retain the non-hydrostatic pressure terms. This approach differs from the development of the Boussinesq equations where pressure is eliminated in favour of high-order velocity and geometry terms. The model gives good results for several test problems including an oscillating basin, propagation of a solitary wave, and a wave transformation over a bar. The hydrostatic and non-hydrostatic versions of the model are compared for a large-scale problem where a fault rupture generates a tsunami on the New Zealand continental shelf. The model efficiency is also very good and execution times are about a factor of 1.8 to 5 slower than the standard shallow water model, depending on problem size. Moreover, there are at least two methods to increase model accuracy when warranted: choosing a more optimal vertical interpolation function, and dividing the problem into layers. Copyright © 2005 John Wiley & Sons, Ltd.

KEY WORDS: finite element; finite volume; wave propagation; non-hydrostatic; free surface; tsunami; dispersive waves

INTRODUCTION

Surface waves have been a focus of interest from very early times—probably prehistoric times. Their seemingly periodic motion at the seashore hides a much more complicated dynamics that

*Correspondence to: Roy A. Walters, National Institute for Water and Atmospheric Research, P.O. Box 8602, Riccarton, Christchurch, New Zealand.
†E-mail: r.walters@niwa.cri.nz

Contract/grant sponsor: Marsden Fund; contract/grant number: 01-NIW013
Contract/grant sponsor: Foundation for Research Science and Technology; contract/grant number: CO1X0024
Contract/grant sponsor: Environment Canterbury

Received 13 December 2004
Revised 17 May 2005
Accepted 24 May 2005

is characteristic of gravity waves. Because modern engineering developments are increasingly concentrated along the coastal margin and thereby subject to wave hazards, there is a need for engineering tools and models to assess wave effects in the range of wave periods from short period wind waves to tides. Hence, much scientific inquiry has gone into this subject.

By their nature, surface gravity waves are dispersive; that is, waves with different frequencies travel at different speeds. For computational efficiency and simplicity, models have tended to cover a small part of the wave spectrum such as models based on the shallow water equations. Peregrine [1] was the first to extend these equations to derive a weakly dispersive model using the Boussinesq equations. More recent research has extended these equations further to include nonlinear and weakly dispersive waves [2, 3]. The basic idea with the Boussinesq equations is to invert the vertical momentum equation to determine pressure, then calculate the horizontal pressure gradients for inclusion into the horizontal momentum equation. This procedure results in a set of equations that resemble the shallow water equations but contain high-order correction terms. There is a significant computational overhead for doing this, approximately an order of magnitude with longer run times.

An alternative method that is pursued here is to retain the vertical momentum equation with the non-hydrostatic pressure. These equations are depth-averaged to yield a set of equations that are similar to the shallow water equations but retain the non-hydrostatic pressure terms. Stelling and Zijlema [4] presented such a scheme using explicit, finite difference methods. In the present paper, a similar method is developed for inclusion into a semi-implicit, finite element coastal ocean model [5]. Other finite element approaches are reviewed in Reference [6].

Of course, the full non-hydrostatic Navier–Stokes equations could be solved directly using z levels [4, 7, 8] or σ levels [9]. However, all these methods require the matrix solution of a three-dimensional pressure Poisson equation which in the end dominates the computational effort. In striving for higher efficiency, the single layer depth-averaged approach is pursued here. The aim here is to examine dispersive surface waves and not consider more complicated internal dynamics such as internal bores.

Overall, the objective of this research is to develop a model that will adequately simulate the dynamics of tsunami propagating across the continental shelf. In practical terms, a large spatial domain with high resolution is required so that source areas and runup areas are adequately resolved. Hence efficiency of the model is a major issue. The ratio of water depth to wavelength (H/L) is typically 0.1 for submarine fault ruptures and 0.4 for submarine landslides. The waves then start as intermediate waves and become shallow water waves as they propagate onshore, and become deep water waves as they propagate offshore.

The model presented here is derived from a general set of three-dimensional hydrodynamic equations. In the following sections, the mathematical and numerical formulations are developed and the results for several examples are presented in order of their computational difficulty.

MATHEMATICAL FORMULATION

The general procedure in this development is to start with the Reynold's averaged Navier–Stokes equations (RANS) and end up with a set of vertically averaged equations similar to the well known shallow water equations but containing extra pressure terms. As will be

seen, the resultant model is almost as efficient as traditional shallow water models but can accommodate dispersive waves.

The initial governing equations are the RANS equation for an incompressible fluid, derived from the Navier–Stokes equations by time-averaging over turbulent time scales to form an equation for the mean value of the dependent variables. The Boussinesq approximation is used so that density variations are included only in the gravity term. The equations are expressed in a rotating frame of reference and the spatial domain includes a free surface. These equations represent a three-dimensional form of the RANS equations that are suitable for geophysical applications. Turbulence closure schemes are not considered here and a general eddy viscosity formulation is employed. For simplicity, density is assumed to be constant.

In tensor form, the equations of momentum and mass conservation are

$$\frac{\partial u_i}{\partial t} + u_j \frac{\partial u_i}{\partial x_j} + 2\varepsilon_{ijk}\Omega_j u_k = -\frac{\partial p}{\partial x_i} - g\delta_{i3} + \frac{\partial}{\partial x_j} A_j \frac{\partial u_i}{\partial x_j} \tag{1}$$

$$\frac{\partial u_i}{\partial x_i} = 0 \tag{2}$$

where the convention is used that repeated indices are summed, x_i, $i = 1, 3$ are distances (x, y, z) along the coordinate axes in the east, north, and upward direction, respectively; $u_j(x_i, t)$, $j = 1, 3$ are velocity components (u, v, w) along the coordinate axes; ε_{ijk} is an alternating tensor [10]; Ω_k are the components of the Earth's angular velocity in the local coordinate system; $p(x_i, t)$ is kinematic pressure; g is gravitational acceleration; δ_{ij} is the Kronecker delta which equals 1 if $i = j$ and 0 otherwise; and A_j are eddy viscosity coefficients.

Pressure is separated into a hydrostatic pressure p_{h} and a dynamic (reduced or non-hydrostatic) pressure $\hat{q}$ such that $p = p_{\mathrm{h}} + \hat{q}$ and by definition

$$\frac{\partial p_{\mathrm{h}}}{\partial z} = -g, \quad \text{or} \quad p_{\mathrm{h}} = p_{\mathrm{a}} + g(\eta - z) \tag{3}$$

where $\eta(x, y, t)$ is the water-surface elevation measured from the vertical datum, and p_{a} is kinematic pressure (atmospheric) at the free surface. In the following, p_{a} is neglected. Introducing these definitions, the governing equations become

$$\frac{\mathrm{D}u_i}{\mathrm{D}t} + 2\varepsilon_{ijk}\Omega_j u_k = -g\frac{\partial \eta}{\partial x_i} - \frac{\partial \hat{q}}{\partial x_i} + \frac{\partial}{\partial x_j} A_j \frac{\partial u_i}{\partial x_j} \tag{4}$$

$$\frac{\partial u_i}{\partial x_i} = 0 \tag{5}$$

where $\mathrm{D}/\mathrm{D}t$ is a material derivative and hydrostatic pressure no longer appears in the vertical momentum equation.

The equation for the free surface η is derived by an integration of the continuity equation over water depth and application of the kinematic free surface and bottom boundary conditions:

$$\frac{\partial \eta}{\partial t} + \frac{\partial}{\partial x}\left[\int_h^\eta u \,\mathrm{d}z\right] + \frac{\partial}{\partial y}\left[\int_h^\eta v \,\mathrm{d}z\right] = 0 \tag{6}$$

where $h(x, y)$ is the land elevation measured from the vertical datum, and $H = \eta(x, y, t) - h(x, y)$ is the water depth. The vertical datum is arbitrary, but is usually set equal to the average water surface elevation (sea level). This choice minimizes truncation errors in the calculation of the water surface gradients.

These equations are solved with subject to conventional boundary conditions that include stress and zero normal flow conditions at solid boundaries, stress and pressure conditions at the free surface, discharge or water-level conditions at river sources, and sea level and radiation conditions at open boundaries. Neglecting atmospheric pressure, $p = \hat{q} = 0$ at the surface and Dirichlet or Neumann conditions on pressure must be specified at open boundaries.

Equations (4)–(6) form a closed system of equations for the five dependent variables u, v, w, η, and $\hat{q}$. At this point, they can be solved in three dimensions using a variety of methods, such as those of Casulli and Zanolli [8] or Stelling and Zijlema [4]. This is the appropriate course of action if the particular problem depends on details of the velocity field or internal dynamics such as density intrusions. However, the interest here is on the propagation of dispersive surface waves for which a depth-averaged formulation is expected to result in a more efficient numerical model.

Depth-averaged equations

The governing equations (4) and (5) are averaged over the water depth to derive a set of governing equations similar to the two-dimensional shallow water equations but containing additional terms. The depth integration will not be repeated here as it appears in many standard references. However, the additional pressure terms will be treated in more detail, as this is the important addition to the standard derivation.

The dynamic pressure is expressed in terms of a horizontal variation and a vertical profile $\hat{q}(x, y, z, t) = q(x, y, h, t) f(z)$. Applying the Leibniz rule, the depth integral of the dynamic pressure gradient in the horizontal momentum equation is

$$\int_h^\eta \frac{\partial \hat{q}}{\partial x_i} \, \mathrm{d}z = \frac{\partial}{\partial x_i} \int_h^\eta \hat{q} \, \mathrm{d}z - \hat{q}_\eta \frac{\partial \eta}{\partial x_i} + \hat{q}_h \frac{\partial h}{\partial x_i} = \frac{\partial}{\partial x_i} q \int_h^\eta f \, \mathrm{d}z + q_h f_h \frac{\partial h}{\partial x_i} \tag{7}$$

where $i = 1, 2$, and $\hat{q}_\eta = 0$. Finally,

$$\int_h^\eta \frac{\partial \hat{q}}{\partial x_i} \, \mathrm{d}z = \frac{\partial}{\partial x_i}(\alpha H q) + q \frac{\partial h}{\partial x_i} = H \frac{\partial}{\partial x_i}(\alpha q) + q \left(\alpha \frac{\partial \eta}{\partial x_i} + (1 - \alpha) \frac{\partial h}{\partial x_i} \right) \tag{8}$$

where the constant α is the vertical average of $f(z)$, and $f_h = f(h) = 1$. In this development, $f(z)$ is taken to be a linear function in order to maintain upward compatibility with linear finite element bases used in the full three-dimensional version of the model. Hence, $\alpha = 0.5$.

Depth-averaging (4) and using (8), the horizontal momentum equation becomes

$$\frac{\mathrm{D}\mathbf{u}}{\mathrm{D}t} + \mathbf{f} \times \mathbf{u} = -g \nabla \eta - \nabla(\alpha q) - \frac{q}{H}(\alpha \nabla \eta + (1 - \alpha) \nabla h) + \frac{1}{H} \nabla \cdot (HA \nabla \mathbf{u}) - \frac{\tau_\mathrm{b}}{\rho H} \tag{9}$$

where $\mathbf{u}$ is the depth-averaged velocity, ∇ is the horizontal gradient operator, and τ_b is bottom friction. Surface stress has been neglected. Bottom friction is written as

$$\frac{\tau_b}{\rho H} = \frac{C_D|\mathbf{u}|\mathbf{u}}{H} = \gamma \mathbf{u} \tag{10}$$

where C_D is a drag coefficient and γ is defined by (10). The free surface equation simplifies to

$$\frac{\partial \eta}{\partial t} + \nabla \cdot (H\mathbf{u}) = 0 \tag{11}$$

Equations (9) and (11) with $q = 0$ form the classical shallow water equations.

Next, the vertical momentum equation in (4) and the continuity equation (5) must be depth averaged to derive governing equations for vertical velocity w and dynamic pressure q. The former is

$$\frac{Dw}{Dt} = \frac{D}{Dt}\left(\frac{w_\eta + w_h}{2}\right) = -\frac{(\hat{q}_\eta - \hat{q}_h)}{H} = \frac{q}{H} \tag{12}$$

where w is the depth-averaged vertical velocity and the vertical viscous terms have been neglected. Using linear interpolation in the vertical, w can be expanded into the second term in (12), where w_h is specified by the kinematic bottom boundary condition.

The vertically integrated continuity equation is expressed as

$$\int_h^\eta \nabla \cdot \mathbf{u}\, dz + w_\eta - w_h = 0 \tag{13}$$

This equation is written in finite volume form when it is discretized.

NUMERICAL APPROXIMATION

The numerical model is a semi-implicit finite-volume/finite element scheme that expresses the momentum equation in a Lagrangian form. Wetting and drying are included in the formulation. This section describes the numerical implementation.

The time stepping approach is a split step method that first solves the equivalent of the shallow water equations to find an approximate solution, then solves for dynamic pressure and corrects the approximate solution. The method of solving the shallow water equations (first step) is described in detail elsewhere [5, 11, 12] and is similar to the methods in Reference [13]. A discussion of the stability of these methods can be found in Reference [14]. As a result, this section presents an overview of the existing model, and focuses on the implementation of the dynamic pressure solution.

The equations are discretized in time using a semi-implicit method such that the equations are evaluated in the time interval ($\Delta t = t^{N+1} - t^N$) where the superscript denotes the time level. The distance through the interval is given by the weight θ.

The equations are approximated using standard Galerkin finite element techniques [5, 11]. The equations are discretized after defining a set of two-dimensional triangular or quadrilateral elements in the horizontal plane. Mixed methods are used such that the elements use

a piecewise constant basis function for η, and a constant normal velocity u_n on each edge with a linear variation within the element [15]. These elements are known as the Raviart–Thomas elements of lowest order.

First step

In the first step of the split step approach, the free surface and horizontal momentum equations are solved without the dynamic pressure terms. The problem then reduces to solving the shallow water equations to find an approximate solution at the new time step.

The free surface equation (11) is expressed in weighted-residual form. Because the basis function for η is a piecewise constant, the continuity equation reduces to a finite volume form that conserves mass both locally and globally:

$$A_e \frac{\partial \eta_e}{\partial t} + \oint_{\Gamma_e} (Hu_n)\, d\Gamma_e = 0 \tag{14}$$

where subscript e denotes the value for a specific element; A_e is the element area; u_n is the normal velocity on a side, positive outwards; and Γ_e is the boundary of the element. The last term has been converted from a divergence form to a line integral using the Gauss divergence theorem.

Using a semi-implicit approach, (14) becomes

$$A_e \frac{\tilde{\eta}_e^{N+1} - \eta_e^N}{\Delta t} + \theta \oint_{\Gamma_e} H^N \tilde{u}_n^{N+1}\, d\Gamma = -(1-\theta) \oint_{\Gamma_e} H^N u_n^N\, d\Gamma \tag{15}$$

which expresses the change in surface elevation as a function of the fluxes through the element sides. The tilde denotes the approximate solution from the first step and the subscript n denotes the component normal to an element side.

The momentum equation (9) is also expressed in weighted-residual form using $\Phi(x, y)$ as the basis function for velocity. Integrating the resultant equation by a mid-side quadrature rule on each element and using the discrete time operator from Equation (15), the momentum equation becomes [5, 11]

$$A\tilde{u}_n^{N+1} = G_n - \theta \Delta t \tilde{N}_n^{N+1} \tag{16}$$

where

$$\begin{aligned} A &= M(1 + \gamma \Delta t) \\ G_n &= Mu_n^* + \Delta t F_n^* - (1-\theta)\Delta t N_n^* \\ \tilde{N}_n &= -\int_\Omega g \nabla_n \Phi \tilde{\eta}\, d\Omega + \oint_\Gamma g \Phi \tilde{\eta}\, d\Gamma \end{aligned}$$

and

$$\mathbf{F}^* = -\int_\Omega \Phi(\mathbf{f} \times \mathbf{u})\, d\Omega - \int_\Omega \nabla\Phi \cdot (A_h \nabla \mathbf{u})\, d\Omega + \oint_\Gamma [\Phi A_h \nabla \mathbf{u} \cdot \hat{\mathbf{n}}]\, d\Gamma$$

$\Phi(x, y, z)$ is the basis function for velocity, A_h is horizontal eddy viscosity, M is the mass matrix given by $M = \int_\Omega \Phi\Phi^T\, d\Omega$, Γ is the boundary of the computational domain Ω, and

the pressure gradient term and the horizontal stress term have been integrated by parts. Note that the term containing $(\nabla H/H)(A_h \nabla u)$ has been omitted for simplicity. The line integrals in these equations provide a convenient means to specify the boundary conditions on η and horizontal stress.

Semi-Lagrangian methods are used in order to take advantage of the simplicity of Eulerian methods and the enhanced stability and accuracy of Lagrangian advection methods [16]. The superscripts $N+1$ and N denote variables evaluated at the fixed nodes in the Eulerian grid at times t^{N+1} and t^N. The superscript $*$ denotes a variable evaluated at time t^N at the foot of the Lagrangian trajectory extending from a computational node. At each time step, the velocity is integrated backwards with respect to time to determine where a particle would be at time t^N in order to arrive at a grid node at time t^{N+1} [16]. The material derivative in Equation (9), the first term, thus has a very simple form.

In order to make the model more efficient, Equation (16) is used to eliminate $\tilde{u}_n^{N+1}$ from the free surface equation (15). The resulting equation is in the form of a wave equation at the discrete level and contains only η at the $N+1$ time level:

$$A_e \tilde{\eta}_e^{N+1} - \theta^2 \Delta t^2 \oint_{\Gamma_e} H^N A^{-1} \tilde{N}_n^{N+1} \, d\Gamma = A_e \eta_e^N - (1-\theta)\Delta t \oint_{\Gamma_e} H^N u_n^N \, d\Gamma - \theta \Delta t \oint_{\Gamma_e} H^N A^{-1} G_n \, d\Gamma \tag{17}$$

In practice, Equation (17) is assembled and solved for $\tilde{\eta}^{N+1}$. Using these results, Equation (16) is solved for $\tilde{u}_n^{N+1}$. The full velocity is recovered by calculating the velocity at the vertices of each element, then interpolating the tangential component of velocity at the midsides.

Note that in the discrete wave equation (17), water depth H is a factor in all the side flux terms. When $H=0$ (i.e. the side is dry), there is automatically no water flux through that side. When all sides of an element are dry, the water level is stationary in time. Hence, wetting and drying are implemented without any special treatment.

Second step

In the second step, the momentum equations are inverted and used to replace u_n and w in the continuity equation. The result is an equation for dynamic pressure q. Finally, u_n and w are back-calculated from the solution for q. Presently, the free surface elevation is not corrected so that $\eta^{N+1} = \tilde{\eta}^{N+1}$.

The vertical velocity w and the dynamic pressure are approximated with piecewise constant bases in the horizontal, the same bases that were used for η. The Galerkin form of the vertical momentum equation then becomes

$$\frac{1}{2}\left[\frac{Dw_\eta}{Dt} + \frac{Dw_h}{Dt}\right] = \frac{q}{H} \tag{18}$$

where w is approximated as a linear function in the vertical and a common factor of A_e has been deleted from the equation. w_h is determined from the kinematic boundary condition at the bottom.

Next, u_n and w are updated with the dynamic pressure terms as

$$u_n^{N+1} = \tilde{u}_n^{N+1} - \Delta t \left(\frac{\partial}{\partial n}(\alpha q^{N+1}) + \frac{q^{N+1}}{H^N} \left(\alpha \frac{\partial \tilde{\eta}^{N+1}}{\partial n} + (1-\alpha)\frac{\partial h}{\partial n} \right) \right) \tag{19}$$

$$w_\eta^{N+1} = \tilde{w}_\eta^{N+1} + \Delta t \frac{q^{N+1}}{H^N} \tag{20}$$

where $\alpha = 0.5$ because linear interpolation functions have been used for dynamic pressure and $\tilde{w}_\eta^{N+1}$ is determined by solving (18) with $q = 0$.

From the kinematic bottom boundary condition,

$$w_h^{N+1} = u_h^{N+1} \cdot \nabla h \quad \text{and} \quad \tilde{w}_h^{N+1} = \tilde{u}_h^{N+1} \cdot \nabla h \tag{21}$$

The continuity equation is expressed as the volume integral of (5) over an element. Hence the surface integral of the horizontal velocity is balanced by the vertical flux as

$$\oint\!\!\!\!\!\!\int_{\Gamma_e} u_n \, \mathrm{d}\Gamma_e + A_e(w_\eta - w_h) = 0 \tag{22}$$

Note that this expression is a direct integral of the flux over the surface of a volume defined by the element. This equation differs from the free surface equation (14) in that the kinematic free surface and bottom boundary conditions are not used.

Next, the expressions for u_n and w are substituted into the finite volume continuity equation evaluated at time $N+1$ to derive an equation for dynamic pressure.

$$\begin{aligned} &\oint_{\Gamma_e} H^N \left(\tilde{u}_n^{N+1} - \Delta t \frac{\partial}{\partial n}(\alpha q^{N+1}) - \Delta t \frac{q^{N+1}}{H^N} \left(\alpha \frac{\partial \tilde{\eta}^{N+1}}{\partial n} + (1-\alpha)\frac{\partial h}{\partial n} \right) \right) \mathrm{d}\Gamma_e \\ &\quad + A_e \left[\left(\tilde{w}_\eta^{N+1} + \Delta t \frac{q^{N+1}}{H^N} \right) - w_h^{N+1} \right] = 0 \end{aligned} \tag{23}$$

which can be rearranged as

$$\begin{aligned} &\oint_{\Gamma_e} \Delta t H \left(\frac{\partial}{\partial n}(\alpha q^{N+1}) + \frac{q^{N+1}}{H} \left(\alpha \frac{\partial \tilde{\eta}^{N+1}}{\partial n} + (1-\alpha)\frac{\partial h}{\partial n} \right) \right) \mathrm{d}\Gamma_e - \Delta t A_e \frac{q^{N+1}}{H} \\ &\quad = \oint_{\Gamma_e} H \tilde{u}_n^{N+1} \, \mathrm{d}\Gamma_e + A_e(\tilde{w}_\eta^{N+1} - w_h^{N+1}) \end{aligned} \tag{24}$$

At this stage of development, w_h^{N+1} is approximated as $\tilde{w}_h^{N+1}$ rather than using (21) and (19). For test cases with a flat bed, this approximation makes no difference because w vanishes at the bottom. For the other test cases, the differences between the estimated and corrected velocities are not sufficiently large to create significant errors. However, this approximation requires further development.

There are three types of boundaries where conditions on q must be specified: land (runup) boundaries, open boundaries with incident waves, and radiating boundaries. The natural

boundary condition for this finite element implementation is $\partial q/\partial n = 0$. This condition is the appropriate condition for land boundaries. For open boundaries with water level specified, $q = 0$ is imposed in the elements along the boundary. Thus the wave enters as a shallow water wave and non-hydrostatic corrections are applied after a one element wide buffer zone. At open boundaries with radiation conditions the same strategy is used. There is a one element wide buffer zone where $q = 0$ and a standard Sommerfeld radiation condition is applied at the boundary. Various numerical tests such as the examples in the results section show that there is no significant reflection from the open boundaries.

These equations are assembled in an element by element order and result in a matrix with five diagonals for quadrilateral elements and four diagonals for triangular elements. For small problems such as the test cases presented in the results, direct solvers can be used such as the frontal solver used here [17]. For larger problems such as the tsunami problem presented in the results, an iterative solver with preconditioner can be used such as a Bi-CG with MILU preconditioner [18, 19].

RESULTS

The model using the hydrostatic approximation has been tested on a variety of problems having analytical solutions or experimental data sets. For instance, see the examples for tidal forcing in a polar quadrant and rectangular bay, and a transcritical flow in Reference [5]. Those results show the general accuracy, efficiency, and robust nature of the model. Here, the depth-averaged non-hydrostatic approach is evaluated using a linear variation in the vertical interpolation for dynamic pressure, q.

The first test case is a sinusoidal oscillation in a closed basin, similar to the test case in Reference [4]. The purpose of this test case is to evaluate the phase speed determined in the model and compare that to the results from wave theory which are given as

$$c = c_{sw}\left(\frac{\tanh(kH)}{kH}\right)^{1/2} \quad \text{and} \quad c_{sw} = (gH)^{1/2} \tag{25}$$

where c is phase speed, k is wavevector and c_{sw} is shallow water phase speed. The basin is 10 m long giving a wavelength of 20 m and the water depth is varied from 1 to 20 m covering the range from shallow to deep water waves. The initial condition is a cosine water level variation with $\eta = 0.1$ at one end of the basin, and the negative of this at the other end of the basin. The basin oscillates with period $T = 2L/c$, where T is period and L is basin length. The basin is discretized with uniform quadrilateral elements with side length of 0.1 m. The time step is 0.01 s.

The results for phase speed are shown in Figure 1, where the solid lines are the results from linear wave theory and the symbols are the results from the model. As may be seen, the model results begin to deviate from theory at about $H/L = \frac{1}{2}$, similar to the range of applicability of Boussinesq models [3, 4]. Moreover, the execution time for the non-hydrostatic model was only 1.8 times that of the shallow water model (the direct matrix solver for q is faster than the iterative solver for η for small problems such as this).

For monochromatic waves, the model results can be improved considerably. The vertical variation in pressure determined by linear wave theory (hyperbolic functions) can be used

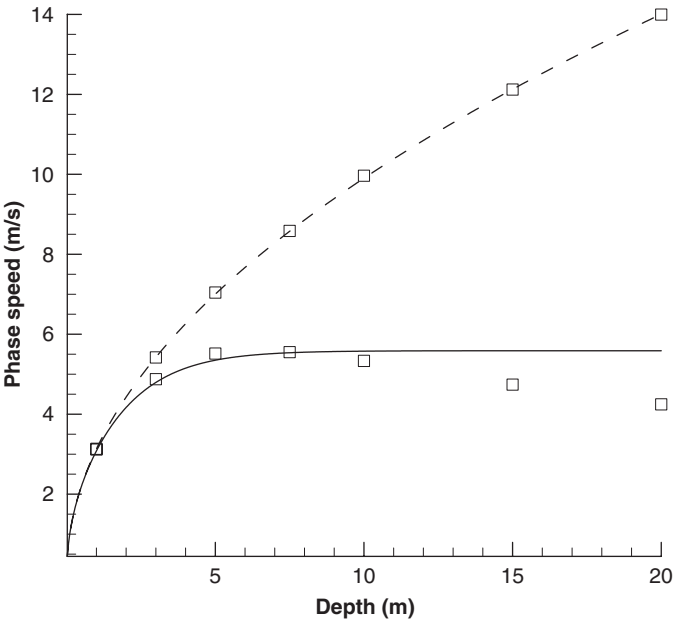

Figure 1. Phase speed as a function of depth, evaluated from the oscillating basin test case. Solid line is phase speed determined analytically from linear wave theory. Dashed line is the phase speed determined analytically for the shallow water limit. Symbols are the phase speed determined from the model for the shallow water equations, and for the non-hydrostatic approximation.

instead of the linear functions used here. However, this approach is only of academic interest because field problems typically exhibit a wide range of wavelengths so that the choice of vertical variation is ambiguous. Nonetheless, there may be other vertical functions that give improved results over the linear functions used here, although compatibility issues between vertical variations in velocity and pressure arise when adopting higher order interpolation schemes. This line of research has not been pursued here.

The second test case is the propagation of a solitary wave along a straight channel with constant depth [4]. This problem is of particular importance for tsunami propagation since these waves can travel long distances as solitary waves. For the test, the initial water surface elevation is given by

$$\eta = A \operatorname{sech}^2 \left[\left(\frac{3A}{4d^3} \right)^{1/2} (x - ct) \right] \tag{26}$$

and the velocity is given in Reference [4] as

$$u = \frac{c\eta}{H} \tag{27}$$

$$w = -z \frac{\partial u}{\partial x} \tag{28}$$

where $A = 2.0\,\mathrm{m}$ is amplitude, d is depth from still water level, and $c = (gH)^{1/2}$. The still water depth is 10 m. The problem is discretized with uniform quadrilateral elements with 1 m side length. The time step is 0.1 s.

With shallow water models, there is an over steepening of the front face of the waves, a reduction in amplitude, and overall unrealistic results. The results of the depth-averaged non-hydrostatic model give excellent results with a maintenance of the waveform, small trailing waves, and small reduction in amplitude (Figure 2).

The third test case is the Beji and Battjes experiment [20] with a wave propagating over a bar in a channel. The bottom topography is shown in Figure 3 where the wave enters from the left, and is dissipated on the slope on the right. The still water depth is 0.4 m and shoals

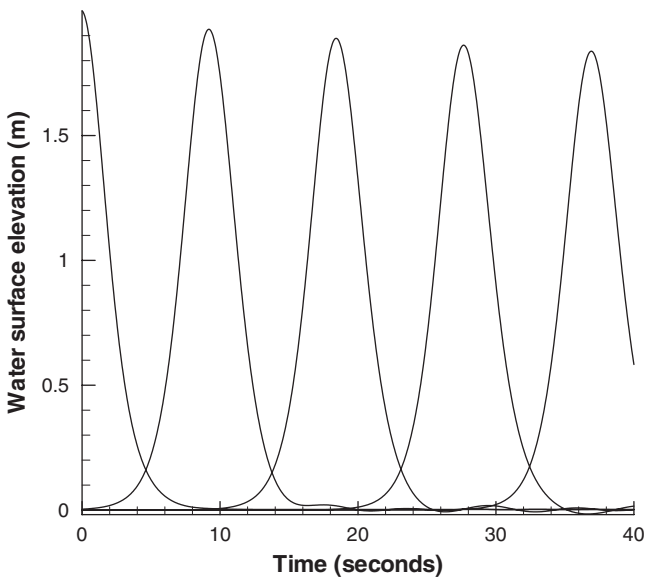

Figure 2. Propagation of a solitary wave along a long channel.

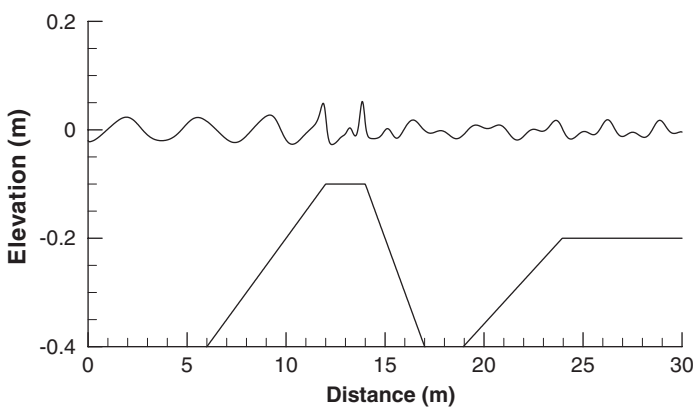

Figure 3. Schematic for the Beji and Battjes experiment. Water level is plotted at 40 s after the start of the experiment. The beach is truncated to allow waves to be radiated from the right boundary.

to 0.1 m over the bar. The front face of the bar has a 1:20 slope and the back side has a 1:10 slope. There is wave absorption on the 1:25 slope that represents a beach. Figure 3 shows the case where the depth at the beach has been limited to 0.2 m in order to apply a radiation condition at the right boundary.

The flume is discretized with regular quadrilateral elements with side length of 0.0125 m. The time step is 0.025 s. The incident wave has an amplitude of 0.01 m and period of 2.02 s. Three methods are used to approximate the beach. One method used a non-absorbing beach where runup and rundown occur. A second method allowed partial reflection from the beach slope by limiting the minimum depth to 0.2 m as the right boundary is approached and applying a radiation condition. A third method used a constant depth of 0.4 m to the right of the bar and the entire wave was radiated. For the first, there were no stability problems with wetting and drying, and the waves were reflected back into the flume causing a modulation of water levels. For the second and third methods, a condition of $q = 0$ (hydrostatic) was specified in the last element and a Sommerfeld radiation condition was applied. This approach performed well without discernable reflected waves.

The model results for the three methods of approximating the beach were compared to the observations. The comparison indicated that there was some reflection from the beach during the experiment, but less than the full reflection from using method 1 and more than full radiation from using method 3. Hence the second method was adopted where there is some reflection from the toe of the beach and the wave is mostly radiated. The results were not found to be sensitive to the exact details of the geometry of the beach.

The results for surface water elevation at 40 s after the experiment started are shown in Figure 3. The waves propagate inward from the left boundary and become steepened and distorted when they encounter the bar. The short wavelength components travel more slowly than the main waveform so they tend to lag. The waves are then propagated as free waves on the back side of the bar and exhibit an irregular wave pattern due to the different phase speeds. As noted by Stelling and Zijlema [4], modelling this pattern correctly places heavy demands on the accuracy of the computed dispersion relation. Furthermore, traditional hydrostatic models give a totally incorrect wave pattern.

The results for the model and the observations at the wave gauges used in the experiment are shown in Figure 4. The model results are reasonably accurate with the largest discrepancies located between the back of the bar and wave absorber (Gauge 9, Figure 4) as would be expected. The source of the discrepancies is not clear. On the one hand, there are uncertainties in the representation of an absorbing beach (see above). On the other hand, there are unknown errors in the model results. In contrast to the representation here, Stelling and Zijlema [4] approximate the beach as a constant depth channel with a sponge layer at the end. Using a two layer approach, their results have about the same accuracy but increased high frequency content as compared to the observations or the results here.

The fourth example is a field-scale problem simulating the propagation of a tsunami generated by a submarine fault rupture on the New Zealand continental shelf. The location of the fault is near the town of Kaikoura on the northeast coast of the South Island of New Zealand (Figure 5). The area is characterized as the convergence zone between the Pacific and Australian plates and the fault is a thrust fault on the continental slope at a depth of about 1000 m. The fault is about 100 km long and 10 km wide, and has a maximum vertical

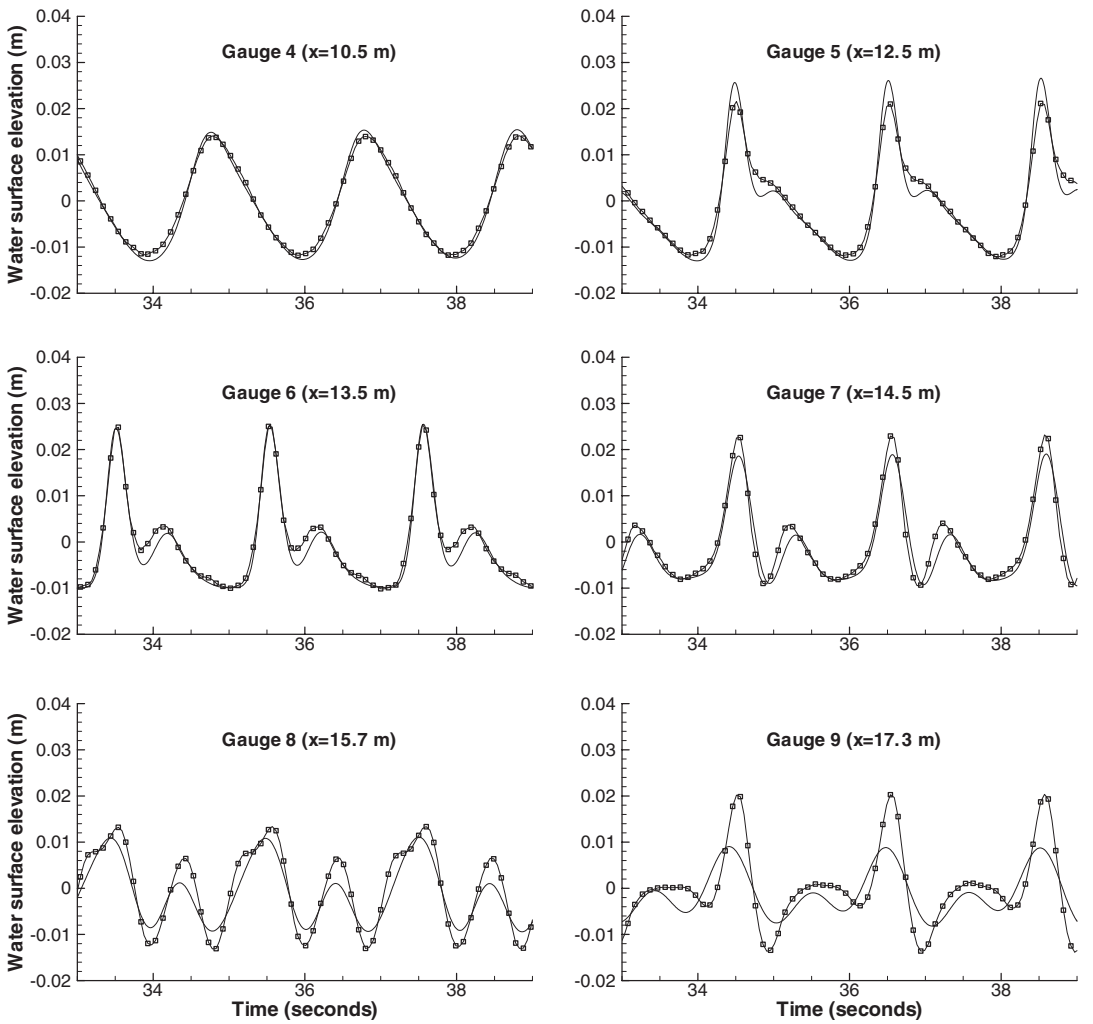

Figure 4. Model results (solid line) and observations (symbols) for the Beji and Battjes experiment.

displacement of 4 m (Figure 6). The fault displacement shown in Figure 6 was used as the initial condition for water surface elevation.

Using the width of the fault displacement as an estimate of wavelength, the depth to wavelength ratio is about 0.1 ($kH = 0.6$) or slightly above the upper limit of shallow water theory. However, the wave contains shorter wavelength components due to an asymmetric distortion on the fault. Hence a basic issue in this simulation is to determine how accurately shallow water models can reproduce a typical fault-generated tsunami.

The model grid was constructed from a NIWA bathymetric data base for the continental shelf and offshore areas, and from a GPS survey of the dry land up to an elevation of 20 m above MSL. The model grid was generated using programs described in Reference [21], and

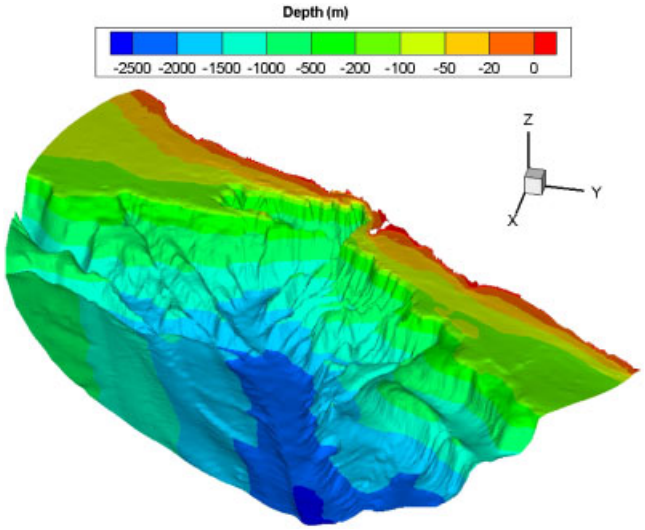

Figure 5. Water depth along the Kaikoura coast. The head of the submarine canyon is at 173.6 E longitude and 42.5 S latitude. For scale, the coastline is approximately 200 km long.

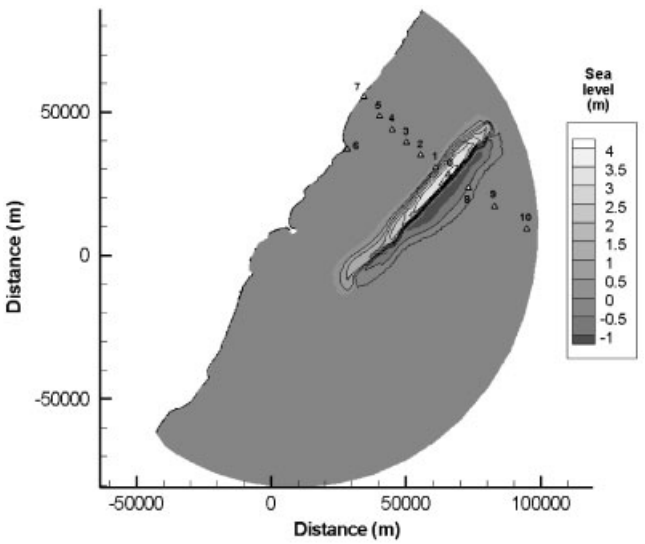

Figure 6. Specified initial water surface elevation. Sites where sea level is plotted in Figures 7 and 8 correspond to the numbered symbols along the path of wave propagation.

contains 513 284 nodes and 1 021 434 triangular elements. Element size varies from about 20 m in the land runup areas, to 400 m near the fault, and to 600 m along the offshore boundary.

The sites identified by symbols in Figure 6 are numerical water level gauges where the results from the various model approximations are compared. For the shoreward propagating

wave, the model results are compared for the shallow water model and the non-hydrostatic model in Figure 7. For the offshore propagating wave, the results are compared in Figure 8.

Initially, the water elevation is specified (Figure 6) and the velocity is zero. This initial condition gives rise to two waves propagating in opposite directions. As the shoreward propagating wave shoals, its speed decreases and its height increases. The differences in the

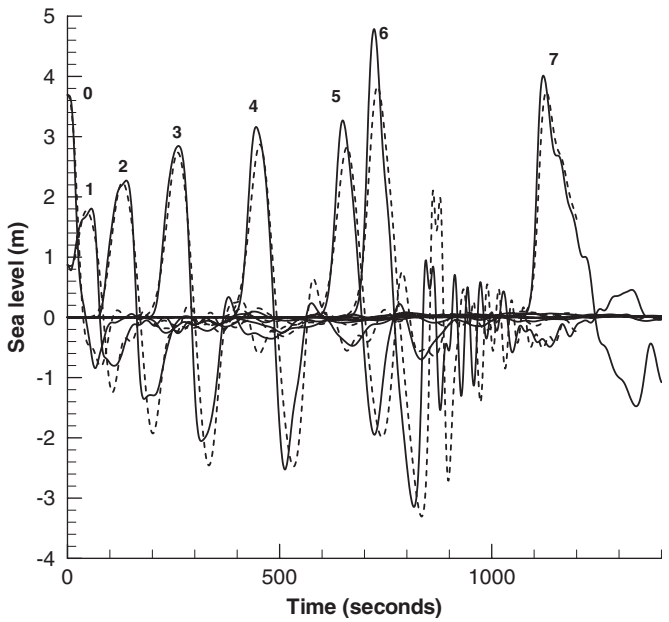

Figure 7. Evolution of shoreward propagating tsunami. Shallow water version (solid), non-hydrostatic version (dashed).

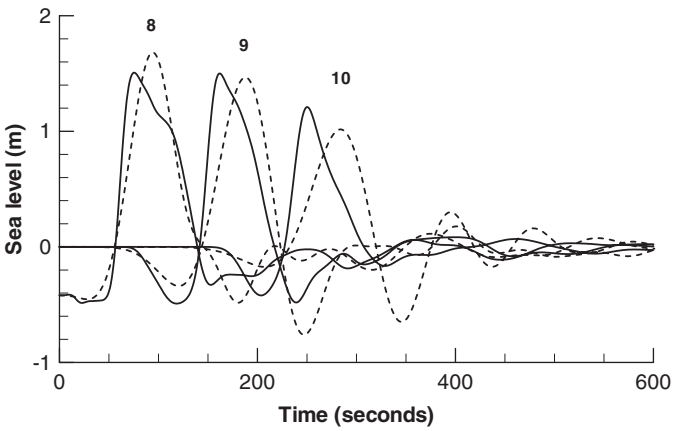

Figure 8. Evolution of offshore propagating tsunami. Shallow water version (solid), non-hydrostatic version (dashed).

results from the shallow water version and the non-hydrostatic version of the model are due to the dispersive nature of the waves (Figure 7). Initially the trailing side of the wave is steeper because of the initial wave shape. For the shallow water version, phase speed is only dependent on the height of the wave so the crest travels faster than the trailing slope and the entire wave steepens on its forward face as it propagates shoreward (from 0 to 6 in Figure 7). For the non-hydrostatic version, the short wavelength components have a slower phase speed and the wave attains a form similar to a solitary wave. At the shoreward site (6 in Figure 7), the wave height is about 20% smaller than the shallow water wave. When the waves have finally steepened into a bore directly inshore from the source area, there is little difference in their shape and the height is less for the dispersive wave (7 in Figure 7).

For the offshore propagating wave, the differences are more pronounced (Figure 8). With the shallow water version of the model, the wave incorrectly maintains a steep leading face because phase speed is only dependent on the height of the wave. With the non-hydrostatic version of the model, the wave evolves toward a shape similar to a solitary wave and the short wavelength components lag behind.

As a result, dispersive effects significantly modify the shape of the tsunami for both the onshore and offshore propagating waves. Depending on location along the shore, the runup may be reduced. However, the tsunami propagating offshore (a remote tsunami at a distant location), is modified considerably by dispersive effects.

CONCLUSIONS

The model presented here meets the objectives of reasonable accuracy, efficiency, and robustness in the simulation of dispersive surface gravity waves. Several test cases were used to evaluate the accuracy of the dispersion relation, including an oscillating basin, solitary wave propagation, and the Beji and Battjes experiment. A field scale simulation of a tsunami generated by a fault rupture showed that dispersive effects are significant, particularly for the offshore propagating wave. Shorter wavelength tsunami such as those generated by submarine landslides would be expected to show even greater effects.

Further research along several lines may improve the model accuracy and performance. First, there may be other vertical approximation functions for pressure that give improved results over the linear functions used here. However, compatibility issues between vertical variations in velocity and pressure arise when adopting higher order interpolation schemes so that this avenue is not straightforward. In the end, the best approach may be to use more vertical layers such as demonstrated by Stelling and Zijlema [4]. Second, better approximation methods may improve the accuracy of the corrected vertical velocity and provide a stable method to correct the sea level solution. Finally, the efficiency of the model depends to a great extent on the efficiency of the iterative matrix solver for dynamic pressure. Any improvements in the solver would directly benefit the model.

ACKNOWLEDGEMENTS

The research was partly funded by the Marsden Fund (01-NIW013) administered by the New Zealand Royal Society and by the Foundation for Research Science and Technology (CO1X0024). The Kaikoura

tsunami study was partly funded by Environment Canterbury. The author also acknowledges the helpful comments from the two anonymous reviewers.

REFERENCES

1. Peregrine DH. Long waves on a beach. *Journal of Fluid Mechanics* 1967; **27**:815–827.
2. Wei G, Kirby JT, Grilli ST, Subramanya R. A fully nonlinear Boussinesq model for surface waves. Part 1. Highly nonlinear unsteady waves. *Journal of Fluid Mechanics* 1995; **294**:71–92.
3. Lynett P, Liu P. A numerical study of submarine-landslide-generated waves and run-up. *Proceedings of the Royal Society of London A* 2002; **458**:2885–2910.
4. Stelling G, Zijlema M. An accurate and efficient finite-difference algorithm for non-hydrostatic free-surface flow with application to wave propagation. *International Journal for Numerical Methods in Fluids* 2003; **43**:1–23.
5. Walters RA, Casulli V. A robust, finite element model for hydrostatic surface water flows. *Communications in Numerical Methods in Engineering* 1998; **14**:931–940.
6. Walters RA, Takagi T. Review of finite element methods for tsunami simulation. In *Long-wave Runup Models*, Yeh H, Liu P, Synolakis C (eds). World Scientific: Singapore, 1997; 43–87.
7. Casulli V. A semi-implicit finite difference method for non-hydrostatic free surface flows. *International Journal for Numerical Methods in Fluids* 1999; **30**:425–440.
8. Casulli V, Zanolli P. Semi-implicit numerical modeling of nonhydrostatic free-surface flows for environmental problems. *Mathematical and Computer Modelling* 2002; **36**:1131–1149.
9. Lin P, Li CW. A σ coordinate three-dimensional numerical model for surface wave propagation. *International Journal for Numerical Methods in Fluids* 2002; **38**:1045–1068.
10. Von Schwind JJ. *Geophysical Fluid Dynamics for Oceanographers*. Prentice-Hall: Englewood Cliffs, NJ, 1980; 307.
11. Walters RA. From river to ocean: a unified modeling approach. *Estuarine and Coastal Modeling*. In *Proceedings of the 7th International Conference*, Spaulding ML (ed.). ASCE: New York, 2002; 683–694.
12. Walters RA. Tsunami generation, propagation, and runup. *Estuarine and Coastal Modeling*. In *Proceedings of the 8th International Conference*, Spaulding ML (ed.). ASCE: New York, 2004; 423–438.
13. Casulli V, Walters RA. An unstructured grid, three-dimensional model based on the shallow water equations. *International Journal for Numerical Methods in Fluids* 2000; **32**:331–348.
14. Casulli V, Cattani E. Stability, accuracy, and efficiency of a semi-implicit method for three-dimensional shallow water flow. *Computers and Mathematics with Applications* 1994; **27**(4):99–112.
15. Raviart PA, Thomas JM. *A Mixed Finite Element Method for 2nd Order Elliptic Problems. Mathematical Aspects of the Finite Element Method*. Lecture Notes in Mathematics. Springer: Berlin, 1977.
16. Staniforth A, Côté J. Semi-Lagrangian integration schemes for atmospheric models—a review. *Monthly Weather Review* 1991; **119**:2206–2223.
17. Walters RA. The frontal method in hydrodynamics simulations. *Computers and Fluids* 1980; **8**:265–272.
18. Barragy E, Carey GF, Walters RA. Application of conjugate gradient methods to tidal simulation. *Advances in Water Resources* 1993; **16**:163–171.
19. Barragy E, Walters RA. Parallel iterative solution for h and p approximations of the shallow water equations. *Advances in Water Resources* 1998; **21**(5):327–337.
20. Beji S, Battjes JA. Numerical simulation of nonlinear waves propagating over a bar. *Coastal Engineering* 1994; **23**:1–16.
21. Henry RF, Walters RA. A geometrically-based, automatic generator for irregular triangular networks. *Communications in Numerical Methods in Engineering* 1993; **9**:555–566.

